Global energy confinement scaling predictions for the kinetically stabilized tandem mirror

J. Pratt and W. Horton
Institute for Fusion Studies, The University of Texas at Austin, Austin, Texas 78712

(Received 29 December 2005; accepted 1 March 2006; published online 25 April 2006)

Transport is studied for the kinetically stabilized tandem mirror, an attractive magnetic confinement device for achieving a steady-state burning plasma. For a magnetohydrodynamic stable system, three different radial transport models with Bohm, gyro-Bohm, and electron temperature gradient (ETG) scaling are derived. As a conservative estimate, numerical coefficients in the models are taken to be consistent with tokamak and stellarator databases. The plug mirrors create an ambipolar potential that controls end losses, whereas radial losses are driven by drift wave turbulence, which lowers the electron temperature through radially trapped particle modes and ETG transport losses. The radial transport equations are analyzed, taking into account the Pastukhov energy and particle end losses. For mirror ratio $R_m=9$ and a large density ratio between plug and central cell regions, there is a high axial ion confinement potential $\phi_i/T_i \gg 1$, as demonstrated in the GAMMA-10 by Cho *et al.* [Nucl. Fusion **45**, 1650 (2005)]. Profiles and total energy confinement times are calculated for a proof-of-principle experiment (length $L=7$ m, central cell magnetic field $B=0.28$ T, and radius $a=1$ m) and for a test reactor facility ($L=30$ m, $B=3$ T, $a=1.5$ m). For these parameter sets, radial loss dominates the end losses except in the low temperature periphery. In the limit of negligible radial losses, ideal ignition occurs at $T_i=7.6$ keV from the two-body power end losses. The transport suppressing rotation rate is well below the sonic value and scales similarly to biased wall rotation rates in the Large Plasma Device experiments [Horton *et al.*, Phys. Plasmas **12**, 022303 (2005)]. Simulation results show that the positive dependence of electron radial transport with increasing electron temperature stabilizes the thermal instabilities giving steady state with $T_i=30-60$ keV and $T_e=50-150$ keV with a fusion amplification Q of order 1.5 to 5.0.
 [DOI: 10.1063/1.2188913]

I. INTRODUCTION

Since the 1950s, mirror machines have been developed as simple, yet elegant plasma confinement devices. Several mirrors (often called plugs or anchors) may be linked together with solenoids in order to reduce troublesome end losses; machines of this sort are called tandem mirrors. In the tandem mirror, axisymmetry eliminates the potentially large radial excursion of guiding center orbits that occurred in the classic quadrupole plugged tandem mirror; it also reduces the technology required to create the high magnetic field for the large-mirror-ratio plugs.[3] End losses in the axisymmetric tandem mirror are reduced further by ambipolar trapping, a consequence of the fact that electrons have higher velocities than ions and hence scatter more rapidly. The scattering time is an approximation for the confinement time, so that initially there is a loss of electrons from the plugs of a tandem mirror. However, as electrons are lost, a net positive charge develops in the plugs to hold them back (electron temperature being much greater than the ion temperature). The formation of this potential $\phi_e>0$ leads to the ambipolar trap. An axisymmetric tandem mirror reactor is thus a compact, high-plasma-pressure fusion reactor with the potential of future extrapolation to direct-energy-conversion units operating on end-loss plasmas. Figure 1 shows the flux surfaces of the tandem mirror and a graph of magnetic field and density levels along the axis of the machine, as conceived in the 1970s and operated at Lawrence Livermore National Laboratory in the 1980s. Figure 2 shows details of the quadrupole mirror fields that are the plugs for the central cell plasma. The peaked plasma density n_p shown in Fig. 1 forms the electrostatic confinement potential $\phi_e=T_e \ln(n_p/n_c)\sim 2T_e$. Thus, the ions in the central cell are confined both by the mirror ratio $R_m=B_p/B_{cc}$ and by the electrostatic potential ϕ_e.

Tandem mirrors still possess some inherent advantages over toroidal confinement geometries as noted by Kadomtsev,[4] "…for an infinite straight cylinder the physics of plasma magnetic confinement looks very attractive from the point of view of controlled nuclear fusion applications. To proceed from the ideal picture of an infinitely long cylinder to a closed toroidal configuration it seems that it would be sufficient to take some section of this cylinder and to bend it into a torus. Unfortunately the bending of the magnetic field strength drastically changes plasma properties." With drift wave confinement radial scaling laws, we show that there are clear advantages for using a tandem mirror that does not possess the curved field lines of the torus. From the particle orbit perspective, it is sufficient to note that it is the poloidal magnetic field that radially confines the trapped particles in a tokamak. Thus, once the central cell magnetic field exceeds the poloidal magnetic field in the tokamak, the radial orbits are smaller and simpler in the central cell plasma. The 3.5-MeV alpha particles have a gyroradius of $\rho_\alpha=9$ cm in the 3 T central cell mirror field. This is smaller than the radial excursions of the alpha particles in an ITER sized

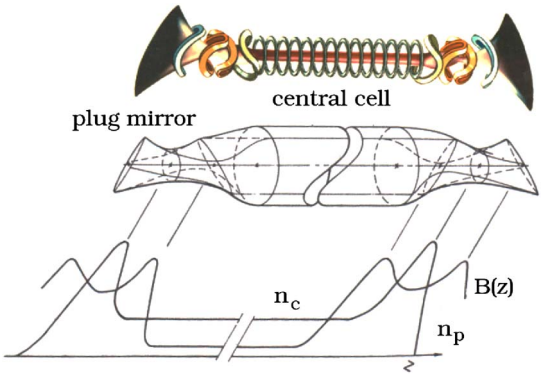

FIG. 1. (Color online) A schematic of the tandem mirror experiment performed in the 1970s from Refs. 7 and 24.

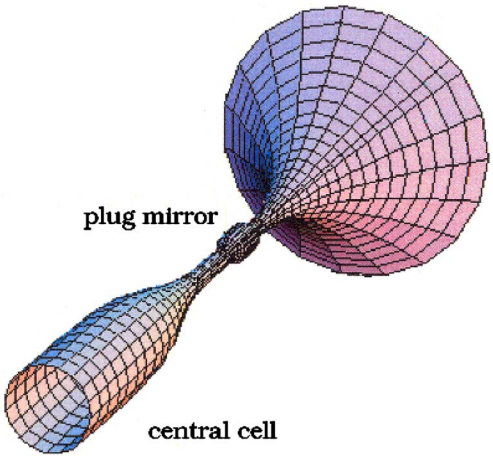

FIG. 3. (Color online) A flux surface of the KSTM from Ref. 7.

device (R/a=6 m/2 m) with 15 MA plasma current and a poloidal circumference of 17 m, giving a poloidal field of roughly 1 T. In a torus, the radial excursions are of order 27 cm with a strong pitch angle dependency; for mirror-trapped alpha particles, the radial excursions are on the order of the alpha gyroradius: 9 cm.

Recent ideas for using kinetic stabilizers provide end plugs that are axisymmetric; this development avoids the geodesic curvature components of the radial excursions that result from the original nonaxisymmetric quadrupole (baseball) end plugs.[5] The kinetically stabilized tandem mirror (KSTM) end plugs may also consume less power than quadrupole plugs and allow a wider range of plug parameters. Figure 3 shows the flux surfaces of the KSTM detailed in Refs. 6 and 7. The power consumed by the kinetic stabilizers has been estimated to be of order 5–10 MW.[8]

In the present work, our goal is to derive scaling laws for the confinement time in the kinetically stabilized tandem mirror for the case when there is anomalous radial transport from drift wave turbulence. Using energy and particle confinement laws, we evaluate the levels of fusion power (P_α) and auxiliary heating (P_{ECH}) required to satisfy Lawson's criterion for fusion and achieve the break-even point for power output.

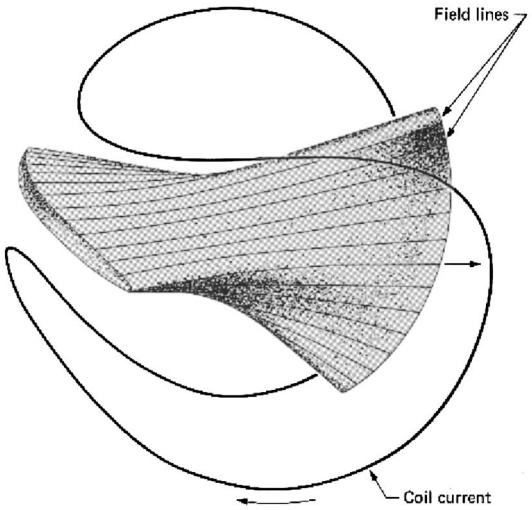

FIG. 2. A close-up of the baseball coils at the ends of the tandem mirror experiment from Ref. 25.

Based on the Bohm, gyro-Bohm, and electron thermal gradient (ETG) turbulent diffusion models, we derive scaling laws for the temperature-power relationship, confinement time, and stored energy. The ETG model is derived from the limit of high $\beta_e m_i/m_e$ in the gyro-Bohm formula; it agrees with the Alcator scaling laws. We then estimate dimensionless transport coefficients for each of these models using a simple matching technique: we match our confinement time scaling laws with a result predicted and experimentally observed for the L97 low-mode scaling in NSTX[9] (National Spheric Torus Experiment) Our scaling laws are then compared with several experimental databases for tokamaks and stellarators, including both low-mode and high-mode machines. The well-known confinement improvement at high β, as well as the absence of destabilizing toroidal curvature, makes the use of the tokamak and stellarator confinement database a conservative radial transport estimate. Finally, we evaluate Lawson's criterion for ignition and determine the temperature at which the KSTM achieves break-even. Results are discussed for a larger fusion reactor version of the KSTM (FR) as well as a smaller proof-of-principle (PoP) KSTM machine. The parameters that define these two machines are summarized in Table I.

The 27 m long GAMMA 10 tandem mirror with confinement potentials of 2 keV has reached ion temperatures of several keV with 200 kW of ion cyclotron heating (ICH) in the central cell and 300–400 kW of electron cyclotron heating (ECH) in the plugs. The central cell exhibits drift wave fluctuations that have been manipulated through the variation of the shearing from the rotational motion due to the radial electric field. The Pastukov end loss formula gives $\tau_\parallel$ =30 ms and the observed end loss confinement time is $\tau_\parallel$ =40 to 45 ms; this is in reasonable agreement with the data.[1] The net radial loss rate of particles is about one-half that of the end loss rate, consistent with the drift wave model for anomalous radial transport. The GAMMA 10 team found that the tandem mirror configuration allows external control of the rotational shearing rate; they theoretically and experi-

TABLE I. Machine parameters.

Parameter	PoP value	FR value	Scale-up (FR/PoP)
a	1 m	1.5 m	1.5
L	7 m	30 m	4.28
n	10^{20} m^{-3}	10^{20} m^{-3}	1
B_{cc}	0.28 T	3 T	10.7
B_{plug}	2.5 T	18 T	7.2
T_e	130 eV	60 keV	461
T_i	32.5 eV	15 keV	461
Gas type	Deuterium	Deuterium and tritium	
Volume	22 m^3	212 m^3	9.6
Surface area	44 m^2	283 m^2	6.4
$c_i=\phi_i/T_i$	5.75	7.8	1.35
$c_e=\phi_e/T_e$	8	8.5	1.06
p_{ECH}	0.8 MW/m^3	0.8 MW/m^3	1
R_m	9	9	1
β_e	0.066	0.27	4

mentally demonstrated a reliable method of suppressing anomalous radial loss rates from drift wave turbulence.[1] The rotation rate is well below the sonic value and scales similarly to biased wall rotation rates in the Large Plasma Device experiments.[2]

The dominant two-body (n^2) Coulomb power loss rate for the KSTM is ion-ion scattering over the potential barrier rather than the brehmstrahlung radiation from electron-ion collisions.[7] Thus, the ideal ignition temperature is shifted up from the classical 4.7 keV value to $T_i=7.6$ keV (and T_e taken to be $4T_i$) as calculated in Sec. III for the KSTM reactor. The ignition temperature is a function of the machine parameters; this higher value of 7.6 keV is determined by the reactivity $\langle\sigma v\rangle$ and the ambipolar electrostatic potential intrinsic to mirror plasma confinement (Ref. 10, pp. 180–184).

Above the ignition temperature, radial losses control the burning plasma properties. Electron thermal diffusivities χ_e from high β_e (the ratio of electron pressure to magnetic pressure) drift wave theory and from experimental databases show the dependence $n\chi_e\sim$const. Historically, this constant $n\chi_e$ dependence is called the Alcator scaling law; it has been observed in many high-density magnetic confinement devices. The Alcator scaling follows most directly from the theory of electron temperature gradient (ETG) turbulence; therefore, we use the ETG model in comparison with Bohm, low-β_e gyro-Bohm, and empirical models for the radial transport studies in Sec. IV.

II. SCALING LAWS

A. Bohm and gyro-Bohm diffusivity

We use the diffusivity as the basis for all of our scaling laws; gyro-Bohm and Bohm theory models are the standard turbulent models for confinement. For PoP parameters and length scale comparable to the radius ($L_{T_e}=a$), we estimate the Bohm and gyro-Bohm diffusivities for low β_e:

TABLE II. Radial transport parameters.

Parameter	PoP value	FR value	Ratio
ρ_s	5.9 mm	13 mm	2.2
c_s	79 km/s	1.5×10^3 km/s	19
a/ρ_s	170	113	0.66
$\rho_s c_s$	464 m^2/s	2×10^4 m^2/s	43
c^B	0.1	0.003	0.03
c^{gB}	18.4	2.8	0.15
c^{ETG}	4.0	0.06	0.015
χ^B	46 m^2/s	60 m^2/s	1.3
χ^{gB}	24 m^2/s	24.3 m^2/s	1
χ^{ETG}	0.1 m^2/s	0.24 m^2/s	2.4

$$\chi^B = c^B\frac{T_e}{B} = c^B\frac{130\text{ V}}{0.28\text{ T}} = c^B 464\text{ m}^2/\text{s} \tag{1}$$

Notice that in the diffusivity relations in Eqs. (1) and (2), we have not yet given values for the dimensionless constants. For high β_e we use the electromagnetic ETG formula for the diffusivity, c^B, and c^{gB}.[11]

$$\chi^{\text{ETG}} = \frac{m_e}{m_i\beta_e}\chi^{gB} = c^{\text{ETG}}\frac{m_e}{m_i\beta_e}\frac{\rho_s}{L_{T_e}}\frac{T_e}{eB} \tag{3}$$

$$= c^{\text{ETG}}\frac{m_e}{m_i\beta_e}\frac{0.0059\text{ m}}{1\text{ m}}\frac{130\text{ V}}{0.28\text{ T}} = c^{\text{ETG}}0.023\text{ m}^2/\text{s}. \tag{4}$$

In Table II we give estimates for the dimensionless constants (c^B, c^{gB}, and c^{ETG}) and evaluate the resulting diffusivities. Our derivation of these coefficients uses the L97 scaling law, normalized to values measured in the NSTX facility, a process fully explained in Appendices A and B. Table II also contains values for the deuterium gyroradius, sound speed, and number of gyroradii within the plasma for an electron temperature length scale comparable to the radius ($L_{T_e}=a$).

B. Temperature scaling laws

To derive scaling laws for temperature T as a function of the steady state power $P=P_{\text{in}}=P_{\text{loss}}=P_{\text{radial}}+P_{\text{end}}$, we use the heat flux equation

$$q = \frac{P_{\text{radial}}}{A} = -n_e\chi\frac{dT_e}{dr} \approx n_e\chi T_e/a. \tag{5}$$

Here, $A=2\pi aL$ is the surface area of the central cell. We also assume that the end loss is less than the radial loss given by the thermal heat flux; this assumption is verified *a posteriori*. We substitute the diffusivity formulas into this equation to obtain three scaling laws:

$$\chi^{gB}\sim c^{gB}a^{-1}B^{-2}T_e^{3/2},\quad \chi^B\sim c^B B^{-1}T_e,$$
$$\chi^{\text{ETG}}\sim c^{\text{ETG}}a^{-1}n^{-1}T_e^{1/2}, \tag{6}$$

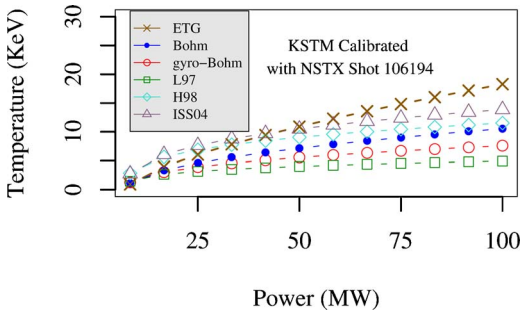

FIG. 4. (Color online) Temperatures T^{gB}, T^{B}, and T^{ETG} versus power for the FR system, compared with empirical predictions. In this graph, the FR achieves $T=12-20$ keV for $P\leqslant 120$ MW. Here the ETG model is the most relevant theoretical model due to the high electron plasma beta.

$$T_e^{gB}\sim\left(\frac{aPB^2}{nL}\right)^{2/5},\quad T_e^{B}\sim\sqrt{\frac{PB}{nL}},\quad T_e^{\mathrm{ETG}}\sim\left(\frac{Pa}{L}\right)^{2/3}. \tag{7}$$

Scaling laws for temperature as a function of steady-state fusion power P, formulated using various thermal diffusivity models (the low-mode L97 law,[12] the high-mode H98 law,[13] and the stellarator law ISS04[14]), are shown in Fig. 4. The models are referenced with a dimensionless diffusivity coefficient such that an electron temperature matching the L97 law (approximately 1.5 keV for the FR) is produced by 3.3 MW of heating for the radial loss channel to match NSTX data.[9] Among our temperature scaling laws (7), the ETG model yields the most favorable temperature for fusion and the gyro-Bohm model the least favorable; this is clearly shown by Fig. 4.

Adopting the tokamak and stellarator confinement databases to predict the radial losses in the central cell of the KSTM has its limitations. The spread in the range of the predicted core temperatures from 5 to 22 keV, shown in Fig. 4, provides an estimate for the range of uncertainty in the predictions based on these empirical (L97, H98, ISS04) and theoretical (ETG, Bohm, gyro-Bohm) laws. The dispersion in predicted temperatures, although wide, is reasonable for the range of input power and confinement laws.

C. Gyro-Bohm and Bohm scaling laws

Stored plasma energy W is defined by the temperatures:

$$W=\int_{\mathrm{Volume}} d^3x\left(\frac{3}{2}\right)n_e(T_e+T_i)$$

$$=\frac{3}{2}n_e(T_e+T_i)V=1.5n_e(T_e+T_i)\pi a^2L, \tag{8}$$

where V is the volume. Here we use the mean value theorem to define the mean temperatures T_e and T_i in Eq. (8) for the stored plasma energy W and confinement time τ_E. At this point, for the sake of clarity, we define new constants $f^{gB}\sim(c^{gB})^{-2/5}$, $f^{B}\sim(c^{B})^{-1/2}$, and $f^{\mathrm{ETG}}\sim(c^{\mathrm{ETG}})^{-2/3}$. Substituting the temperature scaling laws from [Eq. (7)], we obtain scaling laws for W:

$$W^{B}=f^{B}a^2L^{0.5}n^{0.5}B^{0.5}P^{0.5}, \tag{9}$$

TABLE III. Summary of global scaling laws for radial loss times τ_E (s).

$\tau_E^B=0.042$	$B^{1/2}$	$L^{1/2}$	a^2	$n^{1/2}$	$P^{-1/2}$
$\tau_E^{gB}=0.016$	$B^{0.8}$	$L^{0.6}$	$a^{2.4}$	$n^{0.6}$	$P^{-0.6}$
$\tau_E^{\mathrm{ETG}}=0.025$	—	$L^{0.33}$	$a^{2.66}$	n^{1}	$P^{-0.33}$
$\tau_{\mathrm{L97}}=0.010$	$B^{0.99}$	$L^{0.93}$	$a^{1.86}$	$n^{0.4}$	$P^{-0.73}$
$\tau_{\mathrm{H98}}=0.067$	$B^{1.08}$	$L^{0.46}$	$a^{2.44}$	$n^{0.41}$	$P^{-0.69}$
$\tau_{\mathrm{ISS95}}=0.060$	$B^{0.83}$	$L^{0.065}$	$a^{2.21}$	$n^{0.51}$	$P^{-0.59}$
$\tau_{\mathrm{ISS04}}=0.103$	$B^{0.89}$	$L^{0.6}$	$a^{2.33}$	$n^{0.59}$	$P^{-0.64}$

$$W^{gB}=f^{gB}a^{2.4}L^{0.6}n^{0.6}B^{0.8}P^{0.4}, \tag{10}$$

$$W^{\mathrm{ETG}}=f^{\mathrm{ETG}}a^{2.66}L^{0.33}nP^{0.66}. \tag{11}$$

The total energy confinement time τ_E is defined by the power balance equation

$$\frac{\partial W}{\partial t}=P-\frac{W}{\tau_E}, \tag{12}$$

where P is the sum of the alpha particle heating and the radio frequency wave heating powers. At steady state, this gives us expressions for the model global confinement times:

$$\tau_E^{B}=f^{B}a^2L^{0.5}n^{0.5}B^{0.5}P^{-0.5,} \tag{13}$$

$$\tau_E^{gB}=f^{gB}a^{2.4}L^{0.6}n^{0.6}B^{0.8}P^{-0.6}, \tag{14}$$

$$\tau_E^{\mathrm{ETG}}=f^{\mathrm{ETG}}a^{2.66}L^{0.33}nP^{-0.33}. \tag{15}$$

Table III provides a comparison between these τ_E scaling laws and several empirical laws adapted to the tandem mirror. Figure 5 shows the dependence of τ_E on power; Fig. 6 shows the stored thermal energy W.

III. MEASURING SUCCESSFUL FUSION

A. Lawson's criterion

Lawson's criterion is a simple, widely used index of thermonuclear power gain for all confinement devices. For steady-state, magnetic-confinement fusion power, the Lawson criterion is simply $n\tau_E\geqslant 10^{20}$ s/m^3. We evaluate this criterion for the fusion reactor at a variety of auxiliary powers, lengths, radii, and mirror ratios. Figure 7 shows how the

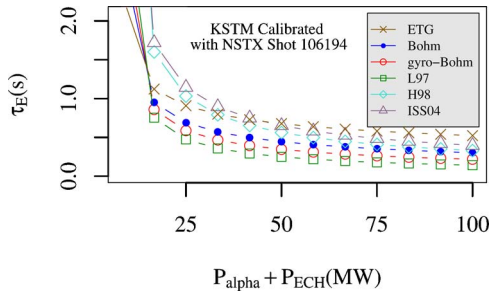

FIG. 5. (Color online) Confinement times, with a variety of scaling laws adopted to the KSTM fusion reactor and the baseline fusion reactor parameters in Table I. Classical drift wave scaling laws (Bohm, gyro-Bohm, and ETG) are normalized to match the empirical L97 results from NSTX at 3.3 MW of radial power loss. At low power, the ISS04 and H98 laws perform best; at high power, the ETG law matches and then exceeds these laws.

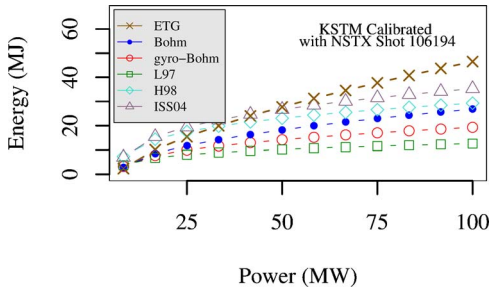

FIG. 6. (Color online) Stored plasma energy with a variety of scaling laws adopted to the KSTM fusion reactor, using the baseline parameters in Table I. Classical drift wave scaling laws (Bohm, gyro-Bohm, and ETG) are normalized to match the empirical L97 results from NSTX at 3.3 MW of radial power loss. Again, we see that the ETG law outperforms all others at high power, while the Bohm and gyro-Bohm stored energy laws give results similar to the L97 low-mode empirical law.

Lawson parameter $n\tau_E$ decreases with input power. The physical reason for this decrease is clear from the derivation of Eqs. (13)–(15). As the input power is increased, the thermal diffusivity increases and thus the energy confinement product $n\tau_E$ decreases.

B. Break-even and ignition in the fusion reactor

Fusion power amplification Q is the usual quantity used to determine the merit of a fusion plasma. The *break-even* condition for fusion is described by the formula[6]

$$Q = \frac{P_{\text{fusion}}}{P_{\text{injected}}} = \frac{5P_\alpha}{P_{\text{external heating}}} = \frac{5P_\alpha}{P_{\text{ECH}} + P_{\text{plug}}} \geqslant 1. \qquad (16)$$

In order to calculate Q for the KSTM, we need to calculate the alpha power from the total injected power. We estimate that half of the central cell volume is burning, $V_{\text{BP}} = (\pi/2)a^2L$, then calculate the alpha power and the break-even point. Figure 8 shows how Q varies with electron temperature; it also shows that break-even ($Q=1$) occurs at approximately $T_e=38.6$ keV, $T_i=9.6$ keV.

The classical ignition temperature $T_i=4.7$ keV is defined by (Ref. 10, pp. 180–184):

$$P_\alpha = P_{\text{brem}} = 5.34 \times 10^{-37} n^2 Z T_e^{1/2} \text{ MW/m}^3. \qquad (17)$$

However, for the tandem mirror, the dominant two-body loss rate is the end loss P_{end} rather than bremsstrahlung power, so that ignition for the KSTM occurs at $P_\alpha = P_{\text{brem}} + P_{\text{end}}$. This raises the ignition temperature from the classical

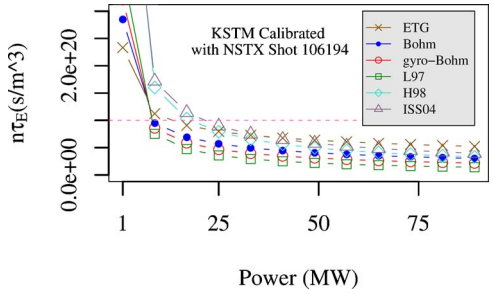

FIG. 7. (Color online) Lawson's parameter $n\tau_E$ for the fusion reactor KSTM as a function of total input power (alpha heating and auxiliary heating).

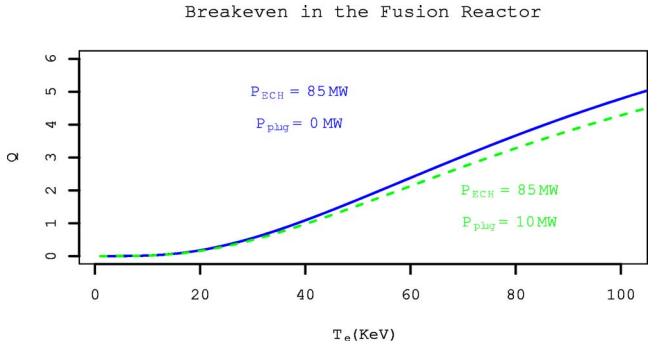

FIG. 8. (Color online) Break-even can be calculated with either injected power or power loss because at steady state these powers are equal. Here we have used P_{ECH} for external heating power; the lower, green line shows Q when power from the plugs is also taken into consideration. Break-even is achieved at $T_e=38.6$ keV, when we have a $P_{\text{ECH}}=85$ MW, and $P_\alpha=17$ MW.

4.7 keV to $T_i=7.6$ keV. Figure 9 shows this shift in ignition temperatures.

Since ignition is a transient state with the total stored plasma energy W increasing with time, the transient Q^* takes into account the power used to increase the plasma thermal energy $W(t)$. Following[15], we define

$$Q^* = 5P_\alpha / \left(P_{\text{ECH}} + P_{\text{plug}} - \frac{dW}{dt} \right) \qquad (18)$$

as the transient fusion power amplification factor.

IV. FUSION POWER AND END LOSSES

We use the Pastukhov tandem mirror end loss time $\tau_\parallel$, experimentally confirmed by Cho *et al.*[1] Axial confinement is determined by ion-ion scattering time τ_{ii}, the plug mirror ratio, and the ambipolar potential

$$\tau_\parallel = \exp(c_i)(A_p c_i \tau_{ii} + R_m L/v_{\text{th},i}), \qquad (19)$$

$$A_p = \frac{\sqrt{\pi}}{4} \frac{R_m}{R_m + 1} \ln(2R_m + 2) = 1.5, \qquad (20)$$

where $R_m = B_{\text{plug}}/B$ is the mirror ratio and A_p is the Pastukhov parameter. Parameters are defined in Table I such that $c_i = \phi_i/T_i = 7.8$, and $c_e = \phi_e/T_e = 8.5$ in order to match

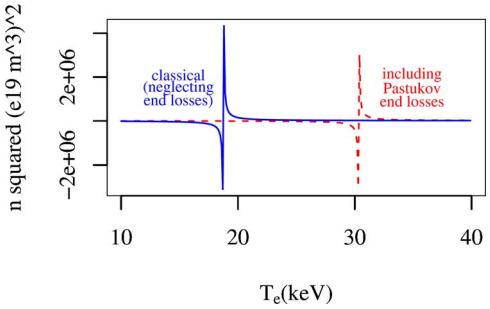

FIG. 9. (Color online) Density vs temperature curves for break-even at steady state. The leftmost singularity (solid curve) shows the ignition temperature without end losses. The rightmost singularity (dashed curve) shows the ignition temperature when end losses are included. The ignition temperature jumps from the classical value of $T_i=4.7$ to 7.6 keV.

TABLE IV. Comparison of loss rates and other variables.

Variable	PoP value	FR value
$\tau_{\parallel}$	0.37 s	796 s
τ_{ii}	4.8 μs	28 ms
ϕ_i	187 eV	117 keV
λ_{Di}	4.2 μm	$9.1\,10^{-5}$ m
$\langle\sigma v\rangle_{DT}$	5.3×10^{-44} m^2	2.7×10^{-22} m^2
$\ln\Lambda_{ii}$	12.6	21.8

with Hua and Fowler.[6] The central cell electron density is denoted by n and the plug density is n_p, given in units of 10^{19} m^{-3}. The practical formula for the ion-ion collision time is

$$\tau_{ii}=1/\nu_i=\frac{66.82\epsilon_0^2 m_i^{1/2}T_i^{3/2}}{n_i e^4\ln\Lambda_i}\sim 5.2\text{ ms}\frac{T_i^{3/2}\text{ keV}}{n_{19}\ln\Lambda_i/20}, \quad (21)$$

using Eq. 11.24 of Goldston and Rutherford.[10] For $n=10^{20}$ m^{-3} and $T_i=10$ keV, we have $\tau_{ii}=4.5$ ms $\gg R_m L/v_{\text{th},i}=0.43$ ms. Further estimates for τ_{ii} are given in Table IV.

Formulas for thermonuclear heating power P_α, radial power loss P_{radial}, and end loss power P_{end} are

$$P_\alpha=n_D n_T\langle\sigma v\rangle_{\text{DT}}E_\alpha=\tfrac{1}{4}n^2\langle\sigma v\rangle_{\text{DT}}E_\alpha, \quad (22)$$

$$P_{\text{radial}}=\frac{3}{2}\frac{n(T_e+T_i)}{\tau_E}, \quad (23)$$

$$P_{\text{end}}=\frac{n(\phi_i+\phi_e)}{\tau_{\parallel}}. \quad (24)$$

Here the alpha particle fusion energy per reaction is $E_\alpha=3.5$ MeV, and we have assumed a 50-50 mixture of deuterium and tritium in our definition of P_α. Contour graphs of these powers versus density and temperature are shown in Fig. 10. The balance between end losses and P_α is shown in Fig. 11. In Eq. (22) the fusion reactivity for deuterium-tritium reactions is defined as

$$\langle\sigma v\rangle_{\text{DT}}=3.68\times10^{-18}T_i^{-2/3}\left[0.5+\left(\frac{T_i}{55}\right)^{1.3}\right]^{-1}\times\exp(-19.94T_i^{-1/3}). \quad (25)$$

The reactivity, Eq. (25), has a maximum of 8.7×10^{-22} m^3/s at $T_i=70$ keV. High plasma pressure in the tandem mirror's central cell causes the resulting diamagnetic currents to deepen the magnetic well self-consistently, thereby increasing the mirror ratio R_m as β_e increases. This is advantageous because the reactor can use the magnetic field to make the system more efficient.

V. COUPLED RADIAL TRANSPORT EQUATIONS

Our goal is to find profiles for n and T_e across the cylindrical region of the KSTM; these profiles can then be used to find regions where Lawson's criterion holds. To do this, we must solve the following system of four coupled differential equations in density and temperature:[6]

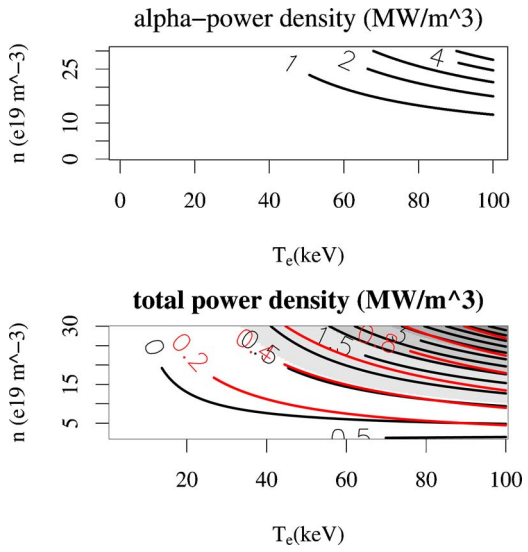

FIG. 10. (Color online) (Above) alpha power density from end losses and (below) ETG radial losses as isolines in units of MW/m^3 in the density-temperature plane. Red lines show contours of β_e.

$$\frac{3}{2}\frac{\partial}{\partial t}n_c T_e+\frac{n_c}{\tau_{\parallel}}(1+c_e)T_e-\frac{1}{r}\frac{\partial}{\partial r}\left(rn_c\chi_e\frac{\partial}{\partial r}T_e\right)=P_e, \quad (26)$$

$$\frac{3}{2}\frac{\partial}{\partial t}n_c T_i+\frac{n_c}{\tau_{\parallel}}(1+c_i)T_i-\frac{1}{r}\frac{\partial}{\partial r}\left(rn_c\chi_i\frac{\partial}{\partial r}T_i\right)=P_i, \quad (27)$$

$$\frac{\partial}{\partial t}n_c+\frac{n_c}{\tau_{\parallel}}-\frac{1}{r}\frac{\partial}{\partial r}\left(rD\frac{\partial}{\partial r}n_c\right)=n_c n_0\langle\sigma v\rangle_{\text{CX}}, \quad (28)$$

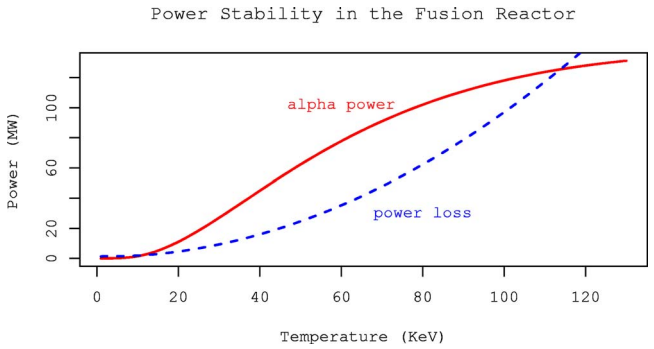

FIG. 11. (Color online) Power balance of the reference reactor as a function of electron temperature at constant density. Here $T_i=0.4T_e$ (for lower T_i these lines do not cross). Fusion alpha power is shown in red and total power loss in blue (dashed). Their intersection at $T_e=11.2$ keV is an unstable fixed point of the ignition dynamics. To the left of this point, power loss is greater than alpha heating power, so that the temperature drops in the absence of auxiliary ECH heating. For temperatures greater than $T_e=11.2$ keV, the alpha power heating exceeds the end loss rate, so that the temperature increases secularly until radial losses that increase with temperature limit the temperature increase to T_e^*. Well above $T_e=11.2$ keV the temperature comes to a new stable equilibrium point. The details of the system's motion about T_e^* depends on whether the radial losses from ETG or Bohm transport balance the alpha heating.[22] For the Bohm radial loss the stable equilibrium temperature is $T_e^*=114$ keV. When the electron temperature is greater than 114 keV the plasma pressure exceeds 1.8 MPa, which is roughly half of the magnetic pressure from $B=3$ T. At still higher temperature, the system disassembles through violent magnetohydrodynamic motions.

$$\frac{\partial}{\partial t}n_p + \frac{n_p}{\tau_p} = n_p N_b \langle \sigma v \rangle_{\mathrm{CX}}. \tag{29}$$

Here the ambipolar potential is $\phi_e = T_e \ln(n_p/n_c)$. In addition, n_0 is the central cell gas feed density and N_b is the density of the neutral beam that drives the plug plasma; both densities are taken to be constants. The exponential buildup of plasma to densities above 10^{20} m^{-3} was demonstrated in the 2XIIB experiment. The charge exchange ionization rate at the neutral beam injection energy is taken as $E_b = 1$ MeV, in accordance with Ref. 6. The particle loss time τ_p is proportional to the ion-electron collision time τ_{ie}, and is defined as

$$\tau_p = \tau_{ie}\frac{n_c}{n_p}\left(1 - \frac{\phi_i + \phi_e}{E_b}\right). \tag{30}$$

Since the charge exchange reactivity $\langle \sigma v \rangle_{\mathrm{CX}}$ is dependent on the ion temperature T_i, the density equations do not decouple from the thermal equations. At this stage, we approximate $\langle \sigma v \rangle_{\mathrm{CX}}$ as a constant. The injected power densities in Eqs. (26) and (27) are

$$P_e = P_{\alpha,e} + P_{\mathrm{ECH}} - Q_{ei}, \tag{31}$$

$$P_i = P_{\alpha,i} + Q_{ei}, \tag{32}$$

where $P_{\alpha,s}$ is the power density transferred into species s from alpha particles, P_{ECH} is the electron cyclotron heating power density, and Q_{ei} is the power transfer from electrons to ions. In the simulations, we use Neumann boundary conditions at $r=0$ and $r=R_{\mathrm{edge}}=\sqrt{2}a$. We absorb the power and particles in the region between a and $\sqrt{2}a$ to represent fast losses to the limiters and to the end loss diverter chambers.

A modified version of the tokamak transport barrier dynamics (TBD) code is used to solve this system of equations. We use boundary conditions of specified edge temperature $T_e(a,t)$ and central cell density $n(a,t)$, with a programmable core rf heating profile $P_{\mathrm{ECH}}(r,t)$.

In the TBD code, we use a modified version of these equations (26)–(29).[16] We let $x=r^2$ in order to simulate in the cylindrical geometry. The Pastuhkov time, a key element for end losses in the KSTM, is dependent on density and temperature, and scales as $\tau_{\parallel} \sim (T^{3/2}/n)$. Here the contribution of ion thermal velocity to $\tau_{\parallel}$ is small in the parameter regime we consider, and is therefore neglected. Figure 12 is a result from our simulation; it shows that the density profile is more peaked than the temperature profile, which reduces the importance of the temperature gradient modes. An adaptive integrater is used with tolerances specified by Ref. 15.

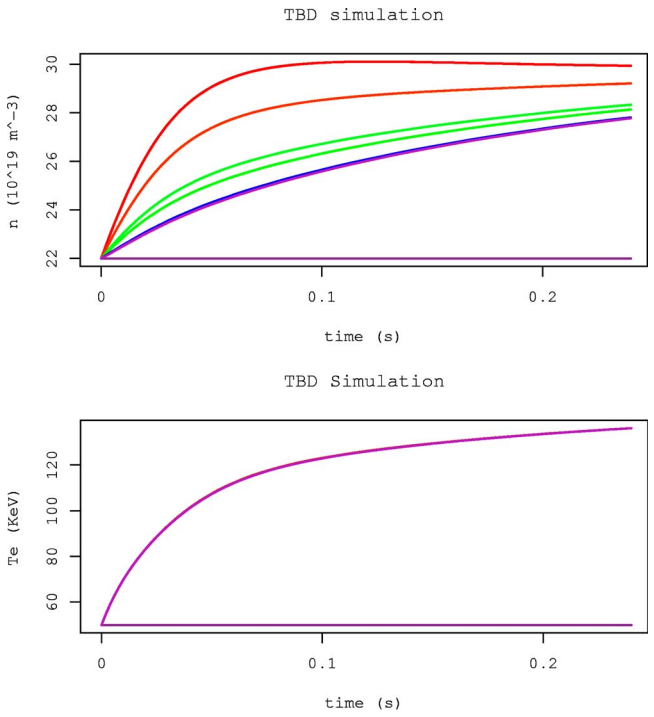

FIG. 12. (Color online) The central cell density (above) and electron temperature (below) as a function of time from the TBD simulation. Density n is in units of 10^{19} m^{-3}. Ten lines are plotted, each for a different radius. Red line is the core density, purple is the edge density, and intermediate midstream lines range between core and edge in ROYGBIV order from top to bottom: Red ($r=0$), pink ($r=0.2$), orange ($r=.4$), yellow ($r=0.6$), light green ($r=0.8$), dark green ($r=1.1$), turquoise ($r=1.3$), blue ($r=1.5$), plum ($r=1.7$), violet ($r=1.9$).

VI. CONCLUSIONS

The tandem mirror offers clear advantages over other fusion devices. The kinetically stabilized tandem mirror is a compact, high power-density fusion reactor based on the axisymmetric tandem mirror, and controlled by external field coils and high energy neutral beams. The operating mode for the KSTM is intrinsically continuous, with no need for rf current drive required by a tokamak reactor. Plasma losses from the ends of the linear system provide the opportunity for coupling the central plasma power generator to a plasma expander chamber for direct conversion to electrical power. Moir *et al.*[17] have outlined how a three-stage "venetian blind" direct energy-convertor could obtain between 60% and 80% efficiency in converting fusion power to electric power. Other uses for the well focused, low entropy, end loss exhaust plasma may be materials testing and environmental clean up.

Two major sources of plasma disruption are eliminated in the tandem mirror that are present in toroidal confinement systems. In the torus, the burning fusion core plasma pressure and pressure gradient are strictly limited by the combination of the pressure gradient in the unfavorable magnetic curvature as measured by $\beta_p = [2\mu_0/B_m^2(r_0)]\int_0^{r_0}(r/r_0)^2 \times(-dp/dr)dr$ when r_0 is the low-order-mode rational surface where $\vec{B}\cdot\nabla\chi_r = 0$. These internal kink modes are driven by both pressure gradient dp/dr and the tokamak toroidal current gradient dJ_ϕ/dr, as shown in Ref. 18. The impact of the sawteeth oscillations on limiting the fusion power in toroidal devices is shown in Ref. 15 using a model from Ref. 19. The sawteeth oscillations are known to trigger the neoclassical tearing modes that produce magnetic islands of the order of a few centimeters in width, for example, in JET,[20] which will also limit the performance of the tokamak reactor.

We use the standard theoretical models for plasma thermal diffusivity and also empirical plasma confinement laws to investigate the fusion power capabilities of the axisymmetric kinetically stabilized tandem mirror proposed by

Post.[5] We find that although the Bohm scaling formula does not allow the system to reach steady-state fusion, the more relevant theoretical diffusivity formula for high $\beta_e \gg 0.1$ derived from electron magnetic drift waves,[11] and the ETG model[21,22] yields a reasonable operating window for a burning plasma with $T_i=30-60$ keV and $T_e=50-150$ keV. The fusion power density, shown in Fig. 10, is $P_\alpha=1-5$ MW/m^3, and for the burning core volume of $V_{\mathrm{BP}}=106$ m^3 $(r<a/2)$, the net fusion power is 100–500 MW. We take the injected power required to maintain the end plugs to be as large as 10 MW,[8] but note that the fusion parameter $Q=P_{\mathrm{fus}}/P_{\mathrm{inj}}$ for the central cell is then between 1.5 and 5.0.

Radial transport simulations indicate that the profiles produced from the alpha particle heating balanced by the radial electron thermal losses are stable to small thermal perturbations. Work continues on determining the profile and amount of auxiliary electron cyclotron heating, P_{ECH}, required to drive and control an attractive burning tandem mirror fusion plasma.

The Bohm, gyro-Bohm, and ETG scaling laws derived specifically for the KSTM give confinement times comparable with those of experimental databases. For the base line FR parameters we estimate break-even at fusion $Q=1$ and $T_e=38.6$ keV; at this temperature, $\tau_E=0.9\pm0.2$ s and $P_\alpha=17$ MW based on the ETG law. Lawson's criterion is achieved for the Bohm law for temperatures less than approximately 28 keV, and for the ETG scaling law for less than 34 keV. Our study projects that the fusion reactor will achieve break-even before reaching the central cell pressure limit. Thus the KSTM appears to provide a viable high power density alternative to the tokamak; as such, it deserves further study. The range of uncertainty of our predictions for KSTM fusion power is evident in Figs. 4–7, which display results for the various scaling laws. Our method adapts the large toroidal confinement databases to theoretical drift wave transport formulas, providing a conservative overestimate of the radial power losses.

This methodology overestimates the amount of radial transport power loss from the drift wave turbulence, and therefore accounts for the lower range of Q $(Q=1-5)$ reported here, compared with $Q_{(H\text{-}F)}=10$ reported in Hua and Fowler.[6] The discrepancy in the Q estimates between these works points to the need for full turbulence simulations and the use of confinement data from the GAMMA-10 device. There is a need for new experiments on large cylindrical plasmas at high temperatures and high plasma pressures.

ACKNOWLEDGMENTS

The authors acknowledge useful discussions with K. Fowler, H. L. Berk, and R. F. Post during the course of this work.

Work supported by DOE Grant No. DE-FG02-04ER5474.

APPENDIX A: ADAPTATION OF THE L97 LAW TO KSTM GEOMETRY

For comparison with Bohm, gyro-Bohm, and ETG confinement time scaling laws [Eqs. (13)–(15)], and in order to determine the dimensionless f constants, we adapt the large, tokamak database low-mode L97 scaling law to the tandem mirror geometry[12] as follows:

$$\tau_E = 0.023 I_p^{0.96} B^{0.03} R^{1.89} a^{-0.06} \kappa^{0.64} n^{0.4} P^{-0.73}. \tag{A1}$$

For the KSTM, we use ellipticity $\kappa=1$, and the approximation $L=2\pi R$. Most importantly, we need to approximate the plasma current I_p in terms of other parameters, since the KSTM has no parallel plasma current running through it. We make the major assumption that the radial confinement in the KSTM is comparable to the confinement in the same size tokamak with the edge safety factor of $q=2$. For a tokamak, τ_E depends principally on the poloidal magnetic field B_p, given by the plasma current I_p in Eq. (A1). We eliminate I_p using a

$$\mu_0 I_p = \int B_p ds = \langle B_p \rangle l, \tag{A2}$$

where $l=2\pi a$ is the poloidal length of the integration path, and taking the edge safety factor

$$q = \frac{B_T a}{\langle B_p \rangle R} = 2. \tag{A3}$$

We calculate the equivalent plasma current I_p, using the fact that $q(a)=2$ to obtain

$$I_p = \frac{\pi}{\mu_0} 10^{-6} \frac{B a^2}{R} = 2.5 \frac{B a^2}{R}, \tag{A4}$$

where I_p is 3.5 MA for the equivalent tokamak with $R/a = 4.77/1.5 = 3.2$. The L97 law [Eq. (A1)], which summarizes confinement times from 13 tokamaks and 2000 high quality documented discharges yields for the same size tandem mirror:

$$\tau_{L97}^{\mathrm{STM}} = 0.01 B^{0.99} L^{0.93} a^{1.86} n^{0.4} P^{-0.73}. \tag{A5}$$

For the FR parameters in Table I with power loss of $P=50$ MW, we find $\tau_{\mathrm{L97}}=0.22$ s from Eq. (A5).

APPENDIX B: DETERMINATION OF DIFFUSIVITY COEFFICIENTS

In the NSTX experiment, shot 106 194, LeBlanc *et al.* report that $P=3.3$ MW and $\tau_E=0.014$ s, which matches the L97 prediction.[9] We require that our Bohm and gyro-Bohm scaling laws for confinement time match the L97 prediction at $P=3.3$ MW as well; this matching determines the diffusivity coefficients. We make an independent estimation of the diffusivity coefficients for the PoP and FR machines, and thus we obtain two sets of predictions for c^B and c^{gB}. For the FR at $P=3.3$ MW level, we find $\tau_{E,\mathrm{L97}}=1.57$ s, and for the PoP machine we find $\tau_{E,\mathrm{L97}}=0.028$ s. Resulting values for the diffusivity coefficients are in Table II.

APPENDIX C: PASTUKHOV LOSS RATE OVER AN ELECTROSTATIC BARRIER IN A MIRROR TRAP

The rate of escape of charged particles from a mirror field with a potential barrier $c=e\phi/T$ and a mirror ratio $R_m=B_{\max}/B_{\min}$ is a complex boundary value problem solved by Pastukhov.[23] The Fokker-Planck equation for $F(v,\mu)$ is solved with the mixed boundary conditions

$$F\left(v^2=\frac{e\phi}{m},\mu=1\right)=0 \quad \text{and} \quad v_0\frac{\partial}{\partial v}F=R_m^{-1}\frac{\partial}{\partial \mu}F \tag{C1}$$

at $v=v_0=\sqrt{e\phi/m}$ and $\mu=v_\parallel/v=\cos(\theta)=1$. The electrostatic loss cone boundary is given by $R\mu^2=R-1+e\phi/mv^2$. In the case of ion-ion collisions, the results for density and energy decay are approximately

$$\frac{d}{dt}n_i=\frac{-2n_i}{\sqrt{\pi}\tau_{ii}}\sqrt{\frac{R_m}{R_m+2}}\frac{\ln(2R_m+2)}{c_i\exp c_i}$$

$$=\frac{-2n_iT_i}{\sqrt{\pi}\tau_{ii}}\sqrt{\frac{R_m}{R_m+2}}\frac{\ln(2R_m+2)}{\exp c_i}, \tag{C2}$$

$$\equiv-\frac{n_i}{\tau_\parallel}\frac{3}{2}\frac{d}{dt}n_iT_i \tag{C3}$$

for large electrostatic confinement potential $c_i=e\phi/T_i\gg 1$. Equations (C1) and (C2) are derived in Ref. 23.

[1] T. Cho, J. Kohagura, M. Hirata *et al.*, Nucl. Fusion **45**, 1650 (2005).
[2] W. Horton, J. C. Perez, T. Carter, and R. Bengtson, Phys. Plasmas **12**, 022303 (2005).
[3] J. Kesner, R. S. Post, B. D. McVey, and D. K. Smith, Nucl. Fusion **22**, 549 (1982).
[4] B. Kadomtsev, *Tokamak Plasma: A Complex Physical System* (IOP, Bristol, 1992).
[5] R. F. Post, LLNL Report UCRL-TR-209615, February 7, 2005.
[6] D. D. Hua and T. K. Fowler, LLNL Report UCRL-ID-204783, June 14, 2004.
[7] T. K. Fowler (personal correspondence).
[8] R. F. Post, T. K. Fowler, R. Bulmer, J. Byers, D. Hua, and L. Tung, Fusion Sci. Technol. **47**, 49 (2005).
[9] B. P. LeBlanc, R. E. Bell, S. M. Kaye *et al.*, Nucl. Fusion **44**, 513 (2004).
[10] R. Goldston and P. Rutherford, *Introduction to Plasma Physics* (IOP, Bristol, 1995).
[11] W. Horton Jr., Phys. Fluids **24**, 1077 (1981).
[12] S. M. Kaye and the ITER Confinement Database Working Group, Nucl. Fusion **37**, 1303 (1997).
[13] G. Becker, Nucl. Fusion **44**, R1 (2004).
[14] H. Yamada, J. H. Harris, A. Dinklage *et al.*, Nucl. Fusion **45**, 1684 (2005).
[15] W. Horton, F. Porcelli, P. Zhu, A. Aydemir, Y. Kishimoto, and T. Tajima, Nucl. Fusion **42**, 169 (2002).
[16] W. Horton and P. Zhu, Phys. Plasmas **7**, 4534 (2000).
[17] R. W. Moir, W. L. Barr, D. J. Bender, R. J. Burleigh, G. A. Carlson, R. S. Devoto, J. N. Doggett, J. H. Fink, G. W. Hamilton, and J. D. Lee, Plasma Phys. Controlled Nucl. Fusion Res. (1976); Proceedings of the Sixth International Conference, Berchtesgaden, West Germany, 6–13 October 1976. Volume 3; (A78-10751 01-75) Vienna, International Atomic Energy Agency pp. 223–235 (1977); (A78-10751 01-75) Vienna, International Atomic Energy Agency, 1977, pp. 223–235.
[18] M. N. Bussac, R. Pellat, D. Edery, and J. L. Soule, Phys. Rev. Lett. **35**, 1638 (1975).
[19] F. Porcelli, D. Boucher, and M. N. Rosenbluth, Plasma Phys. Controlled Fusion **38**, 12 (1996).
[20] T. C. Hender, D. F. Howell, R. J. Buttery, O. Sauter, F. Sartori, R. J. La Haye, A. W. Hyatt, and C. C. Petty, JET EFDA contributors, and the DIII-D team, Nucl. Fusion **44**, 243 (2004).
[21] G. T. Hoang, C. Bourdelle, X. Garbet, G. Giruzzi, T. Aniel, M. Ottaviani, W. Horton, P. Zhu, and R. Budny, Phys. Rev. Lett. **87**, 125001 (2001).
[22] G. T. Hoang, W. Horton, C. Bourdelle, B. Hu, X. Garbet, and M. Ottaviani, Phys. Plasmas **10**, 604 (2003).
[23] V. P. Pastukov, Nucl. Fusion **14**, 3 (1974).
[24] R. H. Cohen, Nucl. Fusion **19**, 1295 (1979).
[25] R. F. Post, Nucl. Fusion **27**, 1579 (1987).